IR−UV Double Resonance Spectroscopy of Acetylene in the $\tilde{A}^1A_u$ $n\nu_3'+\nu_4'$ and $n\nu_3'+\nu_6'$ (n = 2, 3) *Ungerade* Vibrational States†

Miwako Mizoguchi, Nami Yamakita, and Soji Tsuchiya*

Department of Chemical and Biological Sciences, Faculty of Science, Japan Women's University, Mejirodai, Bunkyo-ku, Tokyo 112-8681, Japan

Atsushi Iwasaki, Kennosuke Hoshina, and Kaoru Yamanouchi

Department of Chemistry, School of Science, The University of Tokyo, Hongo, Bunkyo-ku, Tokyo 113-0033, Japan

Received: March 30, 2000; In Final Form: June 1, 2000

The IR−UV double resonance spectroscopy has been applied to observe the rovibronic level system of the *ungerade* $n\nu_3' + \nu_4'$ and $n\nu_3' + \nu_6'(n = 2, 3)$ vibrational states in the $\tilde{A}^1A_g(S_1)$ state of acetylene which are accessible from the selected rotational level J'' of the ν_3'' state in the $\tilde{X}^1\Sigma_u^+$ state. As was reported by Utz *et al.* [*J. Chem. Phys.* **1993**, 98, 2742] for the ν_4' and ν_6' bands, the $n\nu_3' + \nu_4'$ and $n\nu_3' + \nu_6'(n = 2,3)$ states are found to couple with each other by the a- and *b*-axis Coriolis interactions. The rotational analysis is performed taking the Coriolis interactions into account to determine the spectroscopic constants including the vibrational term values. The extent of the Coriolis interactions between $n\nu_3' + \nu_4'$ and $n\nu_3' + \nu_6'(n = 2,3)$ is not so significant as that between ν_4' and ν_6'. This is due to a larger anharmonic coupling of the in-plane *trans*-bending ν_3' mode with the in-plane *cis*-bending ν_6' mode than with the out-of-plane torsion ν_4' mode, which causes a larger energy spacing between the pairs of the interacting levels as the ν_3' quantum number increases. It is also found that most of rotational lines in the $3\nu_3' + \nu_6'$ band split into two or more peaks due to the S_1-T_3 interaction, while such rotational line splittings are not found in the $3\nu_3' + \nu_4'$ band. The present finding that the additional excitation in the out-of-plane torsion (ν_4') mode suppresses the splittings suggests that the S_1-T_3 mixing occurs at the planar C_{2h} or C_{2v} geometry rather than at the nonplanar C_2 geometry which is distorted along the torsional coordinate from the planar geometry.

Introduction

The electronically excited $\tilde{A}^1A_u(S_1)$ state of acetylene has been the focus of a great deal of spectroscopic studies. The $\tilde{A}^1A_u-\tilde{X}^1\Sigma_g^+$ band was analyzed first rovibronically by Ingold and King[1] and Innes,[2] and the equilibrium geometry of acetylene in the $\tilde{A}$ state was determined to be planar and *trans*-bent. Later, Watson et al.[3−5] carried out the detailed rotational analyses of the $\tilde{A}$-$\tilde{X}$ band system of the *gerade* vibrational states composed of the excitations in the C−C stretching (ν_2'), the *trans*-bending (ν_3') and the C−H symmetric stretching (ν_1') modes in the $\tilde{A}$ state, where the ν_1' mode was observed indirectly through the combination bands.

In the $\tilde{A}-\tilde{X}$ transition, only the transitions to the vibrational states with the *gerade* symmetry are allowed from the vibrational ground state in the $\tilde{X}^1\Sigma_g^+$ state. To observe the $\tilde{A}-\tilde{X}$ transition to an *ungerade* vibrational state, Utz *et al.*[6,7] adopted an IR−UV double resonance scheme to excite acetylene in the vibrational ground state in the $\tilde{X}$ state to an *ungerade* vibrational state in the $\tilde{A}$ state; acetylene was excited first to a selected rotational level of the $3\nu_3''$ (ν_3'': C−H antisymmetric stretching mode) vibrational state in the $\tilde{X}$ state by irradiating a near-IR laser pulse, and a further excitation to a rotational level of an *ungerade* vibrational state in the $\tilde{A}$ state was achieved by introducing a UV laser pulse. They observed first the transition to the ν_4' and ν_6' states in which the fundamental frequencies of the torsion (ν_4') mode and the in-plane *cis*-bending(ν_6') mode are very close to each other.[6] They interpreted a rotational structure as that perturbed by a Coriolis interaction between the $\nu_4'(a_u)$ and ν_6' (b_u) vibrational states. They also observed the transition to the ν_5' and $\nu_3' + \nu_5'$ states,[7] where ν_5' represents the antisymmetric C−H stretching mode. On the basis of these observations together with the literature values of the fundamental frequencies of the $\tilde{A}$ state acetylene including its isotopomers, the normal-mode analysis was performed to determine the harmonic frequencies and force constants.[8] The IR−UV double resonance spectroscopy was also applied by Fujii *et al.*[9] to observe transitions to other *ungerade* vibrational states in the $\tilde{A}$ state via the ν_3'' and $\nu_1'' + \nu_3''$ (ν_1'': C−H symmetric stretching mode) in the $\tilde{X}$ state.

The nonadiabatic coupling of the $\tilde{A}$ state with other nearby electronic states together with the predissociation *via* the vibrational states in the $\tilde{A}$ state has also been another focus of the spectroscopic investigations of acetylene. A variety of the experimental evidences for the interactions between the $\tilde{A}$ state and the triplet manifold were reported by the Zeeman quantum beat experiment,[10,11] Zeeman anticrossing (ZAC) spectroscopy,[12,13] and high-resolution spectroscopy.[14] Acetylene in the $\tilde{A}$ state which correlates adiabatically to $C_2H(\tilde{A}^2\Pi) + H$ may predissociate into the ground-state product pair, $C_2H(\tilde{X}^2\Sigma^+) + H$. The threshold energy of the predissociation was obtained by observations of the sudden decrease in the fluorescence quantum yield in an energy region just above the dissociation

† Part of the special issue "C. Bradley Moore Festschrift."

10.1021/jp001215y CCC: $19.00
Published on Web 07/22/2000

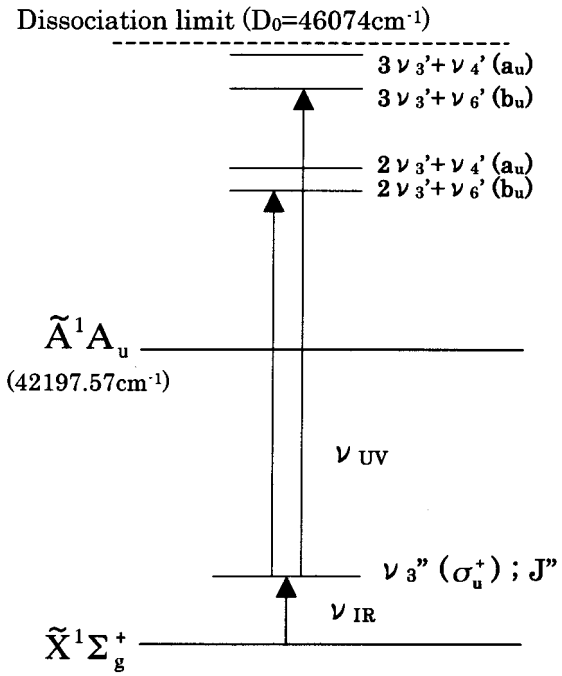

Figure 1. The energy level diagram for the IR−UV double resonance spectroscopy of the $\tilde{A}^1A_u$ $n\nu_3' + \nu_4'$ and $n\nu_3' + \nu_6'$ (n = 2 and 3) states of acetylene.

threshold for $C_2H(\tilde{X}^2\Sigma^+) + H$[15] and the translational energies of the fragment H atom.[16−18] Suzuki and co-workers[19−21] proposed that acetylene in the $\tilde{A}$ state predissociates into $C_2H(\tilde{X}^2\Sigma^+) + H$ *via* the triplet states by detecting the triplet acetylene using the sensitized phosphorescence spectroscopy. This predissociation scheme was supported by the *ab initio* calculations of the potential energy surface by Cui *et al.* [22−23]

In the present study, by means of the IR−UV double resonance spectroscopy, acetylene in the vibrational ground state in the $\tilde{X}$ state is excited to the *ungerade* $n\nu_3' + \nu_4'$ and $n\nu_3' + \nu_6'$(n = 2,3) vibrational levels in the $\tilde{A}$ state *via* selected rotational levels in the ν_3'' state as intermediate levels. We investigate the Coriolis interaction which couples the two vibrational modes of ν_4' and ν_6' in the combination levels of $n\nu_3' + \nu_4'$ and $n\nu_3' + \nu_6'$(n = 2,3) and the vibrational mode dependence of the singlet−triplet interaction appearing as a small splitting only in the $3\nu_3' + \nu_6'$ state.

Experimental Section

The excitation scheme of the IR−UV double resonance spectroscopy is schematically described in Figure 1. Acetylene in the vibrational ground state in the $\tilde{X}$ state was excited first to a single rotational level with a rotational quantum number J'' and a vibrational angular momentum $l'' = 0$ through a P-branch transition of the fundamental absorption band of the antisymmetric C−H stretching mode (ν_3''). Then, the laser-induced fluorescence(LIF) spectrum of the $\tilde{A}^1A_u[n\nu_3' + \nu_4'$and $n\nu_3' + \nu_6'(n = 2,3)$, $J'_{K'_aK'_c}] - \tilde{X}^1\Sigma_g^+[\nu_3'', J'', l'' = 0]$ transitions was measured by scanning the wavelength of the second UV laser. This type of measurements was repeated for the respective selected rotational levels of $J'' = 0-14$ in the ν_3'' vibrational state. The observed LIF spectra from specific J'' levels were composed of a few transitions which were allowed by the rotational selection rule, by which unambiguous rotational assignments could be made.

A sample of acetylene (Takachiho Chemical Co.) was introduced into a stainless steel cell with a pair of Brewster windows and the light baffles at a pressure of around 100 mTorr which was monitored by a diaphragm type pressure gauge (MKS Instruments, 622). Acetylene molecules were excited first by an IR laser pulse (5 ns width, 4 mJ at 3 μm) with a line width of 0.04 cm^{-1} from a single-mode optical parametric oscillator, OPO (Continuum, Mirage 3000) which was pumped by a frequency-doubled injection-seeded Nd:YAG laser (Continuum, Powerlite 8000). After the 5 ns delay from the OPO IR laser, a UV laser pulse which was a frequency-doubled output of the dye laser (Lambda Physik, Scanmate 2EY) pumped by the third harmonics of another Nd:YAG laser (Continuum, Surelite III-10) was introduced into the cell to excite acetylene further from the single J'' rotational level of the ν_3'' state to the rotational levels of the $n\nu_3' + \nu_4'$ and $n\nu_3' + \nu_6'(n = 2,3)$ states in the $\tilde{A}$ state. The fluorescence emitted in a direction perpendicular to the laser beam was collected by a lens system and detected by a solar-blind photomultiplier (Hamamatsu R166UH) through a short-wavelength-cut filter (Sigma-Koki, UTF-28U) to suppress the scattered light of the incident UV laser. The signal was integrated by a boxcar integrator (Stanford Research System, SR 250) and stored in a personal computer after A/D conversion. The resolution of the UV laser was 0.3 cm^{-1} with a grating cavity and 0.1 cm^{-1} with an etalon-inserted cavity. During the IR−UV double resonance experiment, a photoacoustic cell filled with acetylene to a pressure of 3 Torr was irradiated simultaneously with the same OPO IR laser to check the wavelength of the OPO IR laser to be resonant with the respective $P(J'')$ branch lines of the ν_3'' vibrational band.

The wavelength calibration of the visible output of the dye laser was made by the simultaneous measurements of the $^{130}Te_2$ absorption spectrum. In the high-resolution mode using the dye laser with the etalon-inserted cavity, uncertainties associated with the transition wavenumbers were estimated to be $\pm$0.01 cm^{-1}. For the calibration of the low-resolution mode using the dye laser with the grating cavity, the standard spectrum of $^{130}Te_2$ was convoluted by using a Gaussian function with the half-width of 0.15 cm^{-1} to simulate and calibrate the observed absorption spectrum of $^{130}Te_2$. The uncertainties associated with the wavenumber reading of the transition peaks in the low-resolution mode, which were calibrated utilizing the low-resolution $^{130}Te_2$ spectrum, were estimated to be $\pm$0.1 cm^{-1}. This range of the uncertainties was confirmed by comparing the wavenumbers of the same transition peaks of the $\tilde{A}-\tilde{X}$ band of acetylene observed in the high-resolution and low-resolution modes. In the wavenumber region of the dye laser beyond 21200 cm^{-1}, an optogalvanic spectrum of Ne was used for the wavelength calibration. The uncertainties of the wavenumbers of the observed peaks in reference to the Ne standard lines were estimated to be $\pm$0.1 cm^{-1} in the low resolution measurements.

Results and Discussion

IR spectrum of the ν_3'' band. The photoacoustic spectrum of the ν_3'' fundamental band observed using the OPO−IR laser was essentially the same as the high-resolution absorption spectrum reported by Lafferty and Thibault.[24] The rovibrational term value can be calculated on the basis of the reported molecular constants as

$$T(\nu_3'', J'') = \nu_0'' + B_vJ''(J'' + 1) - D_v[J''(J'' + 1)]^2 \quad (1)$$

Close to the ν_3'' state, the $\nu_2'' + \nu_4'' + \nu_5''(\nu_2''$, C−C stretching mode; ν_4'', *trans*-bending mode; ν_5'', *cis*-bending mode) state is located which couples with the ν_3'' state through the 3/245 anharmonic resonance. This coupling is expected to enhance a

Franck−Condon factor of the ν_3' progression in the $\tilde{A}-\tilde{X}$ transition from the ν_3'' state through the contribution of the trans-bending ν_4'' mode.

Selection rule. The selection rule of the transition from a rotational level of the *ungerade* vibrational state in the $\tilde{X}$ state to a rovibrational level in the $\tilde{A}$ state was described previously by Utz *et al.*[6] Briefly, the vibrational selection rule for the $\tilde{A}-\tilde{X}$ transition is $a_g \leftrightarrow a_g$, $a_u \leftrightarrow a_u$, $b_g \leftrightarrow b_g$, $b_u \leftrightarrow b_u$, which is expressed in the reduced C_{2h} symmetry of the $\tilde{A}$ state. Since the Σ_u^+ symmetry of the ν_3'' state correlates to the b_u symmetry of C_{2h}, only the vibrational states in the $\tilde{A}$ state with the b_u symmetry are allowed in the transitions from the ν_3'' state.

Acetylene in the $\tilde{A}$ state is a slightly asymmetric prolate top. Thus, the projection of the total angular momentum on the molecule-fixed symmetry axis, K_a', is a quantum number which characterizes the rotational levels. The $\tilde{A}-\tilde{X}$ band system of acetylene is of the b-type, in which the rotational selection rule is $\Delta J = 0,\pm1$ and $\Delta K_a = K_a' - l'' = \pm1$. The parity selection rules for the $\tilde{A}-\tilde{X}$ transition are: e $\leftrightarrow$ f in the Q-branch, and e $\leftrightarrow$ e, f $\leftrightarrow$ f in the P- and R-branches. Since all of the rotational levels in the ν_3'' level in the $\tilde{X}$ state have e-parity, the levels with f-parity and those with e-parity are accessible through the Q-branch transitions and the P- and R-branch transitions, respectively.

Taking account of the a_u symmetry of the electronic wave function and the a_u symmetry of the ν_4' vibration, the rovibronic parity is defined as $(-1)^{K_C'}$. On the other hand, for the ν_6' vibration with b_u symmetry, the parity is defined as $-(-1)^{K_C'}$. Since $K_a' + K_c' = J'$ or $J' + 1$, the rovibronic parity of the ν_4' and ν_6' states can be determined as follows. In the $K_a' = 0$ levels of the $\nu_4'(a_u)$ state, the parity of the rovibronic level becomes $(-1)^{J'}$, which is *e*-parity. Thus, these levels are accessible only through P- and R-branch transitions from the rotational levels of the ν_3'' state. On the other hand, the rovibronic parity of the $K_a' = 0$ levels of the $\nu_6'(b_u)$ state is $-(-1)^{J'}$, which is *f*-parity, so that only Q-branch transitions are allowed to these levels. In the transitions to the $K_a' = 1$ levels of the $\nu_4'(a_u)$ state, the $J'_{1,J'}$ and $J'_{1,J'-1}$ rotational levels which are the lower and upper components of the *K*-type doubling have *e* and *f* parities to which the P and R-branch transitions and the Q-branch transitions are allowed, respectively. Alternatively, in the transitions to the $K_a' = 1$ levels of $\nu_6'(b_u)$, the $J'_{1,J'}$ and $J'_{1,J'-1}$ rotational levels have *f* and *e* parities to which the Q-branch and the P- and R-branch transitions are allowed.

$2\nu_3' + \nu_4'$ and $2\nu_3' + \nu_6'$ Bands. Figure 2 shows the IR−UV double resonance spectra of the transitions to the $2\nu_3' + \nu_4'$ and $2\nu_3' + \nu_6'$ states in the $\tilde{A}$ state from the selected rotational level J'' of the $\nu_3''(\Sigma_u^+)$ state in the $\tilde{A}$ state which was prepared prior to the rovibronic excitation by the UV laser. The observed wavenumber ν_{UV} of the double resonance spectral peak can be converted to the term value of the rovibronic level in the $\tilde{A}$ state using $T(\nu_3'', J'')$ defined in eq 1 as

$$T_{\nu'} = \nu_{UV} + T(\nu_3'', J'') \tag{2}$$

It is convenient to define the reduced term value by subtracting the average rotational energy $B_{avg}J'(J'+1)$ and the $\tilde{A}-\tilde{X}$ band origin T_0 from the determined term value

$$T_{red} = T_{\nu'} - T_0 - B_{avg}J'(J'+1) \tag{3}$$

which makes the rovibronic term values of a vibronic state having the same K_a to be almost constant against J'. In eq 3, $T_0 = 42197.57\ cm^{-1}$ reported by Van Craen *et al.*[4] and $B_{avg} = 1.074\ cm^{-1}$ adopted by Utz *et al.*[6] are assumed. In Figure 3 the observed reduced term values for the $2\nu_3' + \nu_4'$ and $2\nu_3' + \nu_6'$ states are plotted as a function of $J'(J'+1)$.

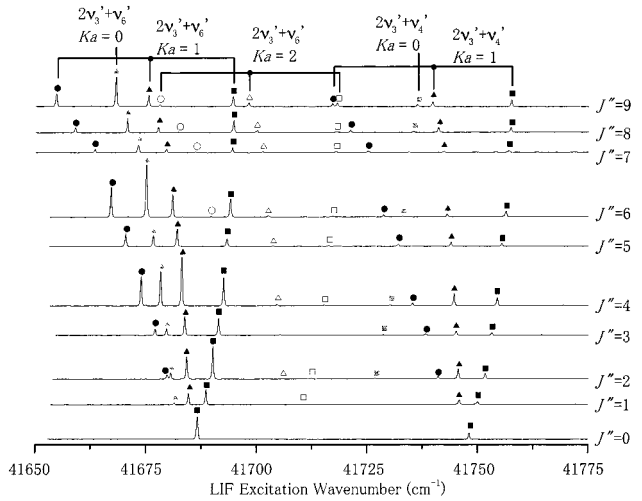

Figure 2. The observed IR−UV LIF spectra of the transitions from the selected rotational levels J'' of the ν_3'' state to the $2\nu_3' + \nu_4'$ and $2\nu_3' + \nu_6'$ vibronic states in the $\tilde{A}$ state. The assignment of the rotational transitions are given as (circle) P-, (triangle) Q-, and (square) R-branch transitions.

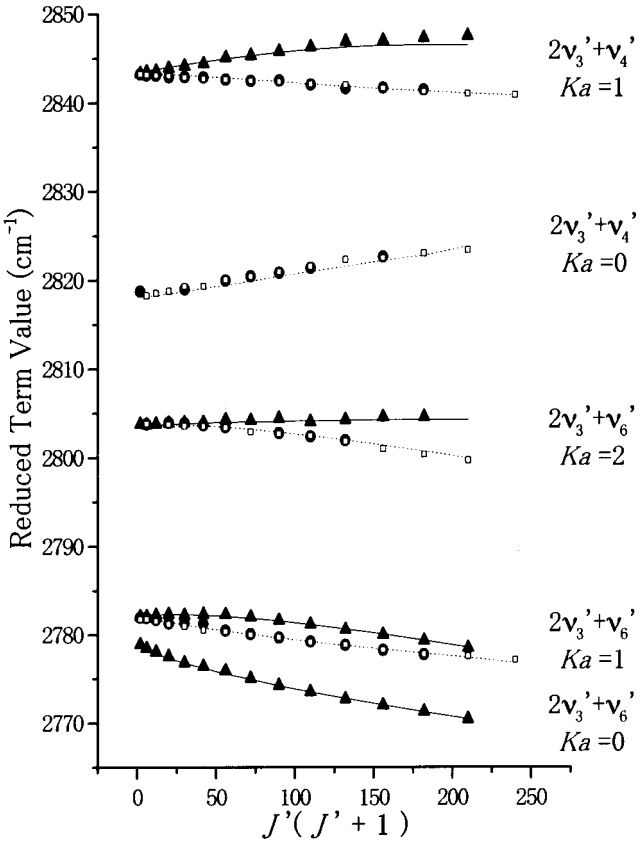

Figure 3. The reduced term value plots of the data given in Figure 2 for the $2\nu_3' + \nu_4'$ and $2\nu_3' + \nu_6'$ states. The circles and squares denote respectively the *f*-parity levels accessible through the P- and R-branch lines, and the triangles the *e*-parity levels accessible through the Q-branch lines. The solid (*e*-parity) and dashed (*f*-parity) curves represent the lines smoothly connecting the term values calculated by the optimized spectroscopic constants determined by the least-squares fits.

In the present energy region, only the $2\nu_3' + \nu_6'(b_u)$ vibrational state is allowed symmetrically from the $\nu_3''(\Sigma_u^+)$ state. In the $\tilde{A}-\tilde{X}$ transition, the rotational transitions to the

$K_a' = 1$ levels are the most intense, and a set of three rotational lines P-, Q-, and R-branches terminating on the $K_a' = 1$ levels as transitions from the corresponding levels in the ν_3'' state. In Figure 2, two sets of strong P-, Q-, and R-branches are identified separated by about 60 cm^{-1} with each other in the low J'' region. We assigned the set of the relatively intense P-, Q-, and R-lines in the lower energy region to the $K_a = 1$ levels of the $2\nu_3' + \nu_6'$ state and the other set in the higher energy region as the forbidden transition to the $K_a = 1$ levels of the $2\nu_3' + \nu_4'$ state which borrows a bright character through the Coriolis coupling with the $2\nu_3' + \nu_6'$ state. As already discussed by Utz *et al.* for the ν_4' and ν_6' bands, the latter forbidden transition is considered to appear due to the Coriolis coupling between these two vibrational states.

The assignments of the P- and R-branch lines were straightforward by application of the combination-difference method because their upper rotational levels have common parities. For the assignment of the Q-branch lines, the reduced term value plot was utilized. In Figure 3 the reduced term value plot of all the observed transitions are shown. The $K_a' = 0$ levels of the $2\nu_3' + \nu_6'$ state have *f* parities for all J' while the $K_a' = 0$ levels of the $2\nu_3' + \nu_4'$ state have *e*-parities for all J'. Therefore, the transitions to the $K_a' = 0$ levels in the $2\nu_3' + \nu_6'$ state are allowed only for the Q-branch, while those in the $2\nu_3' + \nu_4'$ state are allowed only for the P- and R-branches. According to this selection rule, a series starting from the reduced term value of 2779 cm^{-1} composed of only Q-branch transitions, were assigned to the transitions to the $K_a' = 0$ levels of the $2\nu_3' + \nu_6'$state, and a series starting from 2818 cm^{-1} composed of only P- and R-branch transitions were assigned to those of the $2\nu_3' + \nu_4'$ state. In the $K_a' = 1$ series starting from 2843 cm^{-1}, the upper and lower components of the *K*-type doubling were found to have f and e parities, respectively, which supports the assignment that this vibrational state is $2\nu_3' + \nu_4'$ with a_u symmetry. Another $K_a' = 1$ series starting from 2782 cm^{-1} assigned to $2\nu_3' + \nu_6'$ also have a small *K*-type doubling but the upper and lower levels are *f* and *e* parities, which is not consistent with the b_u vibrational symmetry of the $2\nu_3' + \nu_6'$ state. This reversal is ascribable to the strong a-type Coriolis interaction between the $K_a' = 1$ levels of $2\nu_3' + \nu_4'$ and $2\nu_3' + \nu_6'$ states. The energy separation between $K_a' = 0$ series of $2\nu_3' + \nu_4'$ and $2\nu_3' + \nu_6'$ is about 40 cm^{-1} while that of the $K_a = 1$ series is about 61 cm^{-1}, indicating that the $K_a' = 1$ levels of the $2\nu_3' + \nu_4'$ and $2\nu_3' + \nu_6'$ vibrational states repel each other due to a-type Coriolis coupling. In the central wavenumber region of Figure 2, the third set of the P-, Q-, R-branches appears with weaker intensities as the transition from the $J'' \geq 2$ levels in the ν_3'' state. Since the upper and lower components have *f* and *e* parities, these three branches were assigned to the transitions to the $K_a' = 2$ levels of the $2\nu_3' + \nu_6'$ state with b_u symmetry.

Compared the present results with the ν_4' and ν_6' bands observed by Utz *et al.*[6] the sequence of the band origin of the ν_6' state and that of the ν_4' state is reversed, *i.e.*, the band origin of the ν_6' band is located 3.3 cm^{-1} above that of the ν_4' band, while the band origin of the $2\nu_3' + \nu_6'$ band is 39.4 cm^{-1} below that of the $2\nu_3' + \nu_4'$. This can be attributed to the difference in the extent of the anharmonic couplings between the ν_3' and ν_4' modes and that between the ν_3' and ν_6' modes. Another difference between the ν_4' and ν_6' bands and the $2\nu_3' + \nu_4'$ and $2\nu_3' + \nu_6'$ bands can be noted in their intensity partitioning, *i.e.*, the $2\nu_3' + \nu_6'$ band is 2−3 times more intense than the $2\nu_3' + \nu_4'$ band, while the intensities of the ν_4' and ν_6' bands are comparable. This would be caused by the difference in the strength of the Coriolis coupling which mixes the ν_4' and ν_6' modes.

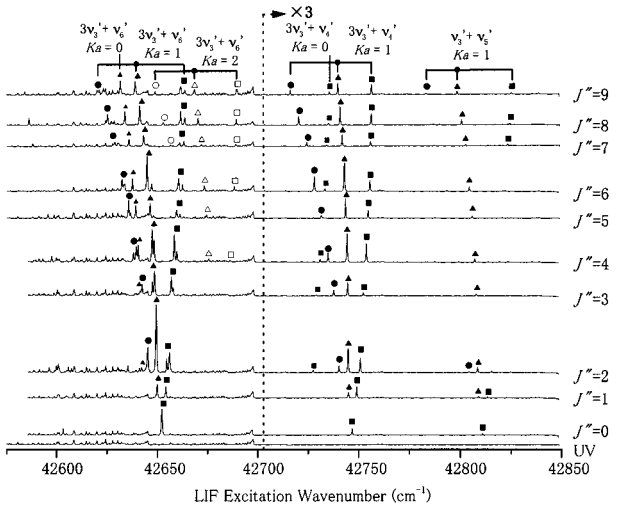

Figure 4. The observed IR−UV LIF spectra of the transitions from the selected rotational levels J'' of the ν_3'' state to the $3\nu_3' + \nu_4'$ and $3\nu_3' + \nu_6'$ vibrational states in the $\tilde{A}$ state. The rotational assignments are given as (circle) P-, (triangle) Q-, and (square) R-branch transitions. The one-photon UV LIF spectrum observed by using the UV laser is given as the lowest spectrum.

$3\nu_3' + \nu_4'$ and $3\nu_3' + \nu_6'$ Bands. In Figure 4 the LIF spectra are shown for the rovibronic transitions to the $3\nu_3' + \nu_4'$ and $3\nu_3' + \nu_6'$ states from the selected J'' rotational levels in the ν_3'' state. In this excitation energy region, besides the IR−UV double resonance spectra, the J''-independent spectral peaks are commonly observed in all the different J'' spectra. These peaks were assigned to the direct one-photon transition peak, because they were exactly the same as those in the UV excitation spectrum shown in the bottom panel in Figure 4. Following the same procedure as taken in the analysis of the $2\nu_3' + \nu_4'$ and $2\nu_3' + \nu_6'$ bands the respective observed peaks were assigned as shown in the reduced term value plots in Figure 5. In the highest wavenumber region of Figure 4, the observed lines were assigned to the rovibronic transitions to the $\nu_3' + \nu_5'$ state. The term values determined from these lines are in accord with those reported by Tobiason *et al.*[7]

The relative line intensities of the $3\nu_3' + \nu_4'$ band is very small compared with those of the $3\nu_3' + \nu_6'$ band. In the $K_a = 1$ lines, the intensity ratios of the $2\nu_3' + \nu_4'$ band to the $2\nu_3' + \nu_6'$ band are around 1/3, while those of the $3\nu_3' + \nu_4'$ band to the $3\nu_3' + \nu_6'$ are less than 1/10, suggesting that the Coriolis interaction is weaker in the $3\nu_3' + \nu_4'$ and $3\nu_3' + \nu_6'$ states. Since the extent of the cross-anharmonicity between the ν_3' and ν_6' modes is larger than that between the ν_3' and ν_4' modes, the $n\nu_3' + \nu_6'$ state is lowered in energy to a larger extent than the $n\nu_3' + \nu_4'$ state when the ν_3' quantum number increases. Consequently, the separation between the band origins of $3\nu_3' + \nu_4'$ and $3\nu_3' + \nu_6'$ (78.8 cm^{-1}) becomes twice as large as that of $2\nu_3' + \nu_4'$ and $2\nu_3' + \nu_6'$ (39.3 cm^{-1}).

It is seen in Figure 4 that some peaks in the $3\nu_3' + \nu_6'$ band split into two or three. These splittings were ascribed to those in the upper levels of the transition on the basis of the combination-difference method as explained in Figure 6. Figure 6, parts a and b, respectively, the double resonance spectra of the $3\nu_3' + \nu_6'$ and $3\nu_3' + \nu_4'$ bands with $K_a = 1$ observed in the high-resolution mode as a function of the term value defined by eq 2. According to the combination-difference relation, the upper level of the R-branch line from the J'' rotational level of

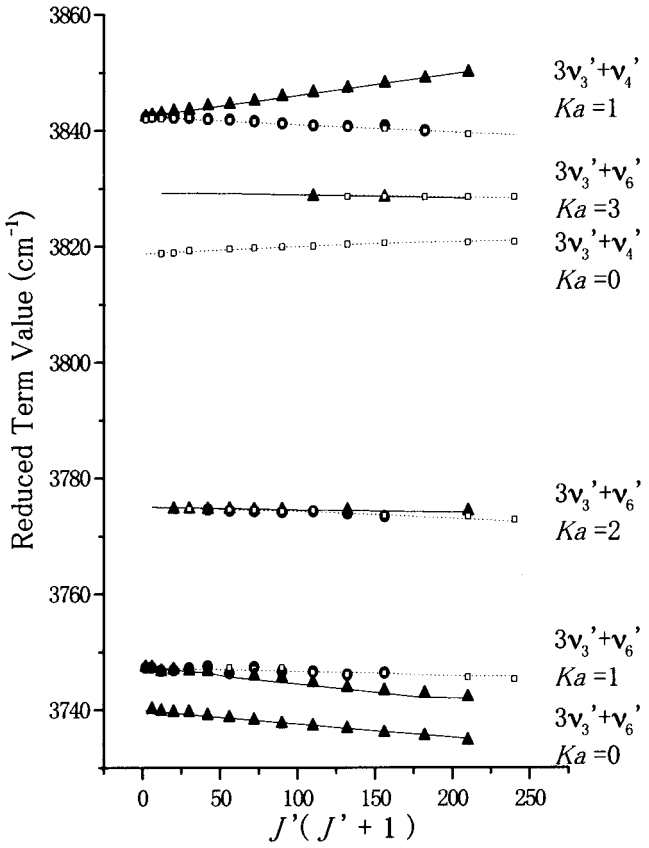

Figure 5. The reduced term value plots of the data given in Figure 4 for the $3\nu_3' + \nu_4'$ and $3\nu_3' + \nu_6'$ states. The circles and squares denote respectively the *f*-parity levels accessible through the P- and R-branch lines, and the triangles the *e*-parity levels accessible through the Q-branch lines. The solid (*e*-parity) and dashed (*f*-parity) curves represent the lines smoothly connecting the term values calculated by the optimized spectroscopic constants determined by the least-squares fits.

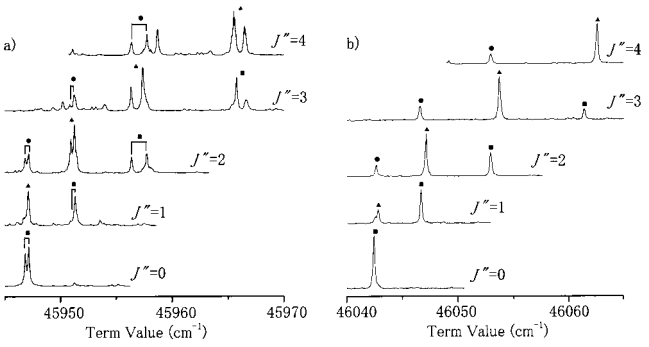

Figure 6. The observed high-resolution IR−UV double resonance spectra of the transitions to the $K_a = 1$ levels of the $3\nu_3' + \nu_6'$ state (a) and those of the $3\nu_3' + \nu_4'$ (b) from the rotational levels J'' of the ν_3'' state as a function of the term value. The P-, Q-, and R-branch lines are specified by circle, triangle and square marks, respectively.

the ν_3'' state is common to that of the P-branch line from the $J'' + 2$ level. As clearly seen in the $3\nu_3' + \nu_6'$ band, the corresponding P- and R-branch lines exhibit the same extent of the line splitting, showing that the upper levels split into two peaks. Contrarily, all of the observed rotational lines in the $3\nu_3' + \nu_4'$ band are composed of single peaks with the spectral width of about 0.1 cm^{-1} which is the laser resolution. Thus, it is concluded that the respective rovibronic levels in the $3\nu_3' + \nu_6'$ state split into two or more levels with separations within about 1 cm^{-1}, while none of the levels in the $3\nu_3' + \nu_4'$ state splits. The splittings identified in the $3\nu_3' + \nu_6'$ state can be attributed to interactions with the triplet levels, which have been identified also in the $3\nu_3'$ and $4\nu_3'$ bands of the $\tilde{A}-\tilde{X}$ transition,[10,11] as discussed later. To deduce the unperturbed term values from the split lines, we define the center-of-lines taking their line positions and the intensities into account.

Rovibronic Analysis of Coriolis-Coupled System. The rotation−vibration Hamiltonian for a nonlinear molecule is described by Watson et al.[25] as

$$\hat{H} = \frac{1}{2}\sum_{\alpha\beta}(J_\alpha - \Pi_\alpha)\mu_{\alpha\beta}(J_\beta - \Pi_\beta) + \frac{1}{2}\sum_k P_k^2 + U + V \quad (4)$$

where J_α and Π_α are the rotational and vibrational angular momenta, respectively, about the α-th axis, in which α and β refer to a molecular axis (*a*, *b*, or *c*), and $\mu_{\alpha\beta}$ is the inverse intertia tensor, and the last three terms represent in their order the kinetic energy, the mass-dependent contribution to the potential energy, and the potential energy of the normal vibrations. The vibrational angular momentum about the α-th axis is defined as

$$\Pi_\alpha = \sum_{rs}\zeta_{rs}^\alpha Q_r P_s \quad (5)$$

where r and s label the normal modes, their coordinates (Q), conjugate momenta (P), and the Coriolis constants ζ_{rs}^α which induces coupling between modes r and s via rotation about α-th axis. The lowest order Coriolis coupling term in the Hamiltonian is

$$\hat{H}_{Cor} = -\sum_\alpha \mu_{\alpha\alpha}^e J_\alpha \Pi_\alpha \quad (6)$$

where $\mu_{\alpha\alpha}^e$ represents a diagonal component of the inverse of inertial tensor at equilibrium geometry. The matrix elements of the Coriolis coupling term were deduced by utilizing the basis functions and the ladder operators proposed by Huber.[26] Due to the symmetry restrictions, the Coriolis couplings about *a*- and *b*-axes mix the $\nu_6'(b_u)$ and $\nu_4'(a_u)$ modes. The selection rules of the rotational levels which interact with each other by the Coriolis couplings in nearly prolate asymmetric rotor was illustrated in Figure 4 of ref 27. The *a*-axis Coriolis coupling mixes the rovibronic levels under the selection rules of $\Delta J' = 0$, $\Delta K_a' = 0$, and $\Delta K_c' = \pm 1$, while the *b*-axis Coriolis coupling mixes the levels under the selection rule of $\Delta J' = 0$, $\Delta K_a' = \pm 1$, and $\Delta K_c' = \mp 1$. The matrix elements of the *a*-axis and *b*-axis Coriolis couplings are given respectively as,

$$\langle \nu_4' = 1, \nu_6' = 0 | \langle J', K_a', K_c' | \hat{H}_{Cor}^a | J', K_a', K_c' \pm 1 \rangle | \nu_4' = 0, \nu_6' = 1 \rangle = -\hbar^2 \zeta_{46}^a \left(\sqrt{\frac{\omega_4}{\omega_6}} + \sqrt{\frac{\omega_6}{\omega_4}} \right) K_a A_e \quad (7)$$

$$\langle \nu_4' = 1, \nu_6' = 0 | \langle J', K_a', K_c' | \hat{H}_{Cor}^b | J', K_a' \mp 1, K_c' \pm 1 \rangle | \nu_4' = 0, \nu_6' = 1 \rangle = \mp \frac{1}{2}\hbar^2 \zeta_{46}^b \left(\sqrt{\frac{\omega_4}{\omega_6}} + \sqrt{\frac{\omega_6}{\omega_4}} \right) \sqrt{(J' \mp K_a')(J' \pm K_a' + 1)} B_e \quad (8)$$

where A_e and B_e are the equilibrium rotational constants about *a*-axis and *b*-axis, respectively, and ω_4 and ω_6 are the harmonic frequencies of the ν_4' and ν_6' normal mode, respectively. In the present fit, $A_e = 13.057$ cm^{-1} and $B_e = 1.12382$ cm^{-1} reported by Watson *et al.*[3] and $\omega_4 = 764.90$ cm^{-1} and $\omega_6 = 768.26$ cm^{-1} reported by Tobiason *et al.*[7] were adopted.

TABLE 1: Optimized Spectroscopic Constants (in cm^{-1}) of $n\nu_3' + \nu_4'$ and $n\nu_3' + \nu_6'$ (n = 0, 2, 3) States of Acetylene

level	ν_4' [a]	ν_6' [a]	$2\nu_3' + \nu_4'$	$2\nu_3' + \nu_6'$	$3\nu_3' + \nu_4'$	$3\nu_3' + \nu_6'$
T_v [b]	42962.26(8) [42962.47(6)]	42966.22(10) [42965.83(9)]	45015.64(10)	44976.33(8)	46016.33(9)	45937.55(7)
A_v	11.12(3) [11.36(5)]	15.08(13) [14.59(13)]	12.50(14)	18.30(4)	17.96(13)	15.24(3)
B_v	1.1453(10) [1.1425(15)]	1.1004(8) [1.1031(15)]	1.1423(13)	1.1119(22)	1.1240(9)	1.1219(8)
C_v	1.0337(3) [1.0323(15)]	1.0259(7) [1.0274(15)]	1.0231(9)	1.0204(8)	1.0240(8)	1.0238(7)
ζ^a	0.696(1) [0.7074(13)]		0.9851(32)		0.9395(38)	
ζ^b	0.719(3) [0.6999(28)]		0.6070(49)		0.7085(41)	
σ_{fit}	0.297 [0. 104]		0.236		0.261	

[a] The values in "[ ]" are those of ref 6. [b] T_0 = 42197.57(1) cm^{-1} given in ref 3.

By treating acetylene in the $\tilde{A}$ state as a rigid asymmetric rotor, the observed term values of the $n\nu_3' + \nu_4'$ and $n\nu_3' + \nu_6'$ (n = 2,3) bands were simultaneously fitted by the least-squares analysis with 10 independent parameters: the two sets of three rotational constants, the two Coriolis coupling constants, ζ_{46}^a and ζ_{46}^b, and the two band origin wavenumbers. The fits were performed with the standard deviations of 0.236 and 0.261 cm^{-1} for n = 2 and 3, respectively. The optimized parameters are listed in Table 1. The term values calculated for respective rotational levels by use of the determined spectroscopic constants are plotted in Figures 3 and 5 for the $2\nu_3' + \nu_4'$ and $2\nu_3' + \nu_6'$ states and $3\nu_3' + \nu_4'$ and $3\nu_3' + \nu_6'$ states, respectively. It is seen from these figures that the agreement of the observed and calculated term values are satisfactory.

In the fit, the centrifugal distortion terms were not included. To test this rigid-rotor approximation, we performed the least-squares fit to the observed transition wavenumber data for the ν_4' and ν_6' bands reported by Utz et al.,[28] and the resulting spectroscopic constants are given in Table 1. Even though the fit was made for the high J' levels (J' = 7−19), the determined constants are in agreement with the corresponding constants derived previously by taking account of the centrifugal distortion effect. In the $n\nu_3' + \nu_4'$ and $n\nu_3' + \nu_6'$ (n = 2,3) bands, the observed rotational levels are limited to the low J' numbers up to 14, so that the neglect of the centrifugal terms is considered to be appropriate.

The sum rule of the Coriolis coupling constants for the $\tilde{A}^1A_u$ acetylene[3] is described as

$$(\zeta_{46}^a)^2 + (\zeta_{46}^b)^2 = 1 \qquad (9)$$

In the present fit without the centrifugal distortion terms, the Coriolis coupling constants determined for the ν_4' and ν_6' states from the data of Utz *et al.*[6] satisfies this rule. However, the Coriolis constants derived for the $n\nu_3' + \nu_4'/\nu_6'$ states listed in Table 1 do not satisfy this rule, i.e., $(\zeta_{46}^a)^2 + (\zeta_{46}^b)^2 = 1.3$ for both n = 2 and 3. It is probable that the deviation from the Coriolis sum rule is caused by the existence of another Coriolis interaction with the third level which perturbs $n\nu_3' + \nu_6'$ and/or $n\nu_3' + \nu_4'$ levels. This possibility is supported by the fact that the A rotational constants given in Table 1 exhibit an irregular dependence on the ν_3' quantum number, suggesting the existence of at least an additional a-axis Coriolis interaction.

A possible perturber for the $2\nu_3' + \nu_4'$ and $2\nu_3' + \nu_6'$ levels is the ν_5' level which is located only 39 cm^{-1} above the $2\nu_3' + \nu_4'$ level and could be coupled through the a-axis Coriolis interaction between the ν_4' and ν_5' modes. Similarly, for the $3\nu_3' + \nu_4'$ and $3\nu_3' + \nu_6'$ levels, the $\nu_3' + \nu_5'$ levels, which is located 76 cm^{-1} above the $3\nu_3' + \nu_4'$ level, is a possible perturber through the a-axis Coriolis interaction. However, as has been suggested by Tobiason *et al.*[7] in the analysis of the ν_5' band, it is also possible that the 5/336 type anharmonic resonance could couple ν_5' and $2\nu_3' + \nu_6'$ in the $2\nu_3' + \nu_4'/\nu_6'$ manifold, and $\nu_3' + \nu_5'$ and $3\nu_3' + \nu_6'$ in the $3\nu_3' + \nu_4'/\nu_6'$ manifold. At this stage, it is uncertain which of these two interactions, *i.e.*, the Coriolis interaction and the 5/336 anharmonic interaction, have a dominant contribution to the $n\nu_3' + \nu_4'/\nu_6'$ manifold. It can be said that at least the ν_5' and $\nu_3' + \nu_5'$ states need to be taken into account for more precise deperturbation.

TABLE 2: The Observed Band Origin Wavenumbers (in cm^{-1}) of the $n\nu_3' + \nu_4'$ and $n\nu_3' + \nu_6'$(n = 0−3) States of Acetylene Measured from the Electronic Term Value T_0 = 42197.57 cm^{-1}

n	$n\nu_3'$ [a]	$n\nu_3' + \nu_4'$	$(n\nu_3' + \nu_4') - (n\nu_3')$	$n\nu_3' + \nu_6'$	$(n\nu_3' + \nu_6') - (n\nu_3')$
0 [b]	0	764.90	764.90	768.26	768.26
1 [c]	1047.55	1799.32	751.77	1785.53	737.98
2	2077.71	2818.07	740.36	2778.76	701.05
3	3081.14	3818.76	737.62	3739.98	658.84

[a] Reference 3. [b] Reference 6. [c] Our unpublished results.

The vibrational term values of the $n\nu_3'$, $n\nu_3' + \nu_4'$, and $n\nu_3' + \nu_6'$ states are listed in Table 2 together with the ν_4' and ν_6' mode frequencies which are defined as $T_0(n\nu_3' + \nu_4') - T_0(n\nu_3')$ and $T_0(n\nu_3' + \nu_6') - T_0(n\nu_3')$, where T_0 represents the vibrational term value of the level specified in the parenthesis. The frequencies of the ν_4' and ν_6' modes decrease as n increases, and this tendency is attributed to the anharmonic coupling with the ν_3' mode. Considering that the decrease of the ν_6' frequency are more prominent than the ν_4' frequency, it can be said that the extent of the anharmonic coupling between ν_3' and ν_6' modes is much larger than that between ν_3' and ν_4'. This may be reasonable because both ν_3' and ν_6' modes are the in-plane vibrations, while ν_4' mode is the out-of-plane vibration which is a motion perpendicular to the ν_3' vibration.

Singlet−Triplet Coupling. Ochi and Tsuchiya[10,11] identified the splittings of the rotational transitions in the $3\nu_3'$ and $4\nu_3'$ bands of the $\tilde{A}-\tilde{X}$ transition. On the basis of the measurement of the Zeeman quantum beat in the fluorescence decay profiles, from which large g-factors were determined, they concluded that the spin−orbit interaction induces the splitting in the rotational structure. Furthermore, through the identification of the zero-field quantum beat which could be achieved only by a considerably high level density, it was suggested that the triplet manifold couples with the vibrationally highly excited region of the electronic ground states.

Field and co-workers[12] recorded the Zeeman anticrossing spectra of the $\tilde{A}$-$\tilde{X}$ transition and reported that the level density near the $3\nu_3'$ band derived from the ZAC experiment was two-orders of magnitude higher than that estimated from the three low lying triplet states, *i.e.*, T_1, T_2, and T_3, and the triplet manifold needs to be coupled with the vibrationally highly excited region of $\tilde{X}\,\Sigma_g^+(S_0)$. They suggested that the intersystem crossing from S_1 to the triplet manifold occurred near the trans-to-cis isomerization barrier on the triplet surface where the overlap of the vibrational wave functions increases to induce an efficient S_1-T_n ($n = 1$ or 2) transition.

To investigate theoretically the characteristic $S_1-T_n-S_0$ coupling occurring in the $3\nu_3'$ and $4\nu_3'$ band of acetylene, ab initio MO calculations were performed.[22,23,29] Schaefer and co-workers[29] calculated the energies of the transition states for the *trans*-to-*cis* isomerization reaction on the T_1, T_2, and T_3 surfaces and concluded by considering the vibrational Franck−Condon overlap that the triplet state which is coupled first by the S_1 electronic state is the T_3 state in the geometry near the half-linear configuration where the trans-to-cis isomerization barrier exists. On the other hand, Morokuma and co-workers[22,23] investigated the dissociation mechanism based on minima on the seam of surface crossing and suggested that the S_1-T_3 transition occurs through the C_2 geometry promoted by the torsional mode. Therefore, the $S_1-T_3-S_0$ mechanism has been supported so far by the experimental and theoretical studies. Later the singlet−triplet mixing was further confirmed experimentally by Suzuki and co-workers[19−21] and Field and co-workers.[30−31]

However, consensus has not been reached whether the S_1-T_3 transition proceeds through the planar geometry, which includes a quasi-linear configuration, or the C_2 geometry which is distorted from the planar configuration along the torsion mode. As has been identified first by Ochi and Tsuchiya, the S_1-T_3 mixing appears as splitting in the rotational structure of the $3\nu_3'$ and $4\nu_3'$ bands. So far, such splittings in the excitation spectrum have been identified only in the $3\nu_3'$ and $4\nu_3'$ bands. In the *ungerade* manifold which becomes accessible in the present IR−UV excitation scheme, $3\nu_3' + \nu_4'$, $3\nu_3' + \nu_6'$, and $\nu_3' + \nu_5'$ are located higher in energy than the $3\nu_3'$ band. Because the *trans*-to-*cis* isomerization barrier is considered to be located near the $3\nu_3'$ state, it is worthwhile to investigate the splittings in the rotational structure of these three vibronic bands.

As shown in Figure 6, part a, splittings whose magnitude is as large as 1 cm^{-1} are clearly observed in the rotational structure of the $3\nu_3' + \nu_6'$ band. On the other hand, the $3\nu_3' + \nu_4'$ band appearing through the Coriolis interaction with the $3\nu_3' + \nu_6'$ level does not exhibit any splittings. In the rotational structure of the $\nu_3' + \nu_5'$ band, the splittings are not identified either. As has been discussed previously, the $3\nu_3'$ vibrational wave function could have large enough overlap with the wave function of the T_3 state near its *trans*-to-*cis* barrier. The present finding that there is no rotational splitting in the $\nu_3' + \nu_5'$ band suggests that the extent of the spread of the $\nu_3' + \nu_5'$ wave function along the ν_3' coordinate is so small that a sufficient overlap with the triplet wave function is not realized near the isomerization barrier.

The remarkable finding is that the $3\nu_3' + \nu_4'$ band does not exhibit the splitting while the $3\nu_3' + \nu_6'$ band does. Considering that these two states are closely spaced with each other and that they have commonly three quanta in the ν_3' mode, both of these bands are expected to exhibit rotational splittings due to the S_1-T_3 interaction. Because the ν_3' mode and the ν_6' mode are the in-plane modes on the C_{2h} plane, the excitation of the ν_6' mode in addition to the $3\nu_3'$ excitation still keeps the vibration on the C_{2h} plane. On the other hand, the ν_4' mode is the out-of-plane mode and the excitation along the torsional ν_4' mode changes the vibrational symmetry with respect to the C_{2h} plane from even to odd. Therefore, the suppression of the rotational splitting at the $3\nu_3' + \nu_4'$ band suggests that the overlap with the triplet manifold becomes significantly small upon the excitation of one quanta in the ν_4' mode, indicating that the triplet manifold has the planar configuration, which includes the quasilinear configuration at the interaction region and the integration along the ν_4' coordinate decreases the S_1-T_3 mixing significantly.

According to the previous theoretical calculation, the S_1-T_3 transition occurs either at the quasilinear geometry or the C_2 geometry distorted along the torsional motion. The present observation that the ν_4' excitation suppresses the S_1-T_3 transition could be regarded as a first experimental evidence that the S_1-T_3 transition proceeds at the planar (C_{2h} or C_{2v}) geometry rather than the C_2 geometry.

Conclusion

(1) The IR−UV double resonance spectra of the *ungerade* $n\nu_3' + \nu_4'(a_u)$ and $n\nu_3' + \nu_6'(b_u)$ ($n = 2$ and 3) states of acetylene were measured *via* the ν_3'' state in the electronic ground $\tilde{X}$ state. From the analysis of the rotational structure, it was found that the $n\nu_3' + \nu_4'$ and $n\nu_3' + \nu_6'$ states couple with each other by the *a*-axis and *b*-axis Coriolis interactions in a similar manner as the ν_4' and ν_6' states.[6]

(2) The rovibronic term values of the $n\nu_3' + \nu_4'$ and $n\nu_3' + \nu_6'$ states were simultaneously fitted by the least-squares analysis by taking account of the Coriolis coupling between these two states. Though the fits were performed with only small residuals, the determined Coriolis parameters and the *A* rotational constants suggested that another Corioris and/or anharmonic interactions exist with a nearby state. The candidates of the secondary perturber for the $n = 2$ and $n = 3$ manifold were estimated to be the ν_5' and $\nu_3' + \nu_5'$ states, respectively.

(3) In the rotational structure of the $3\nu_3' + \nu_6'$ band measured with high-resolution, most of the transition to the $K_a = 1$ rotational levels split into two or more, while those in the $3\nu_3' + \nu_4'$ band did not exhibit any splitting. The splittings in the $3\nu_3' + \nu_6'$ band were interpreted as those caused by the singlet−triplet (S_1-T_3) interaction in a similar manner as the splittings in the $3\nu_3'$ and $4\nu_3'$ bands in the *gerade* manifold. The finding that there is no rotational splitting in the $3\nu_3' + \nu_4'$ band suggested that the out-of-plane ν_4' torsional mode suppresses the singlet−triplet interaction. Therefore, it was inferred that the singlet−triplet mixing occurs at the planar (C_{2h} or C_{2v}) geometry rather than at the C_2 geometry deformed from the planar form along the torsional coordinate.

Acknowledgment. N.Y. and S.T. acknowledge a partial support for the present work by a Grant-in-Aid from Ministry of Education, Science, Culture and Sports (Contracts 11740334 and 11640515). The authors at The University of Tokyo thank the CREST (Core Research for Evolutionary Science and Technology) fund from Japan Science and Technology Corporation. The authors thank Professor F. F. Crim for his sending to us a copy of a part of the Thesis of Dr. A. L. Utz.

References and Notes

(1) Ingold, C. K.; King, G. W. *J. Chem. Soc.* **1953**, 2702.
(2) Innes, K. K. *J. Chem. Phys.* **1954**, *22*, 863.
(3) Watson, J. K. G.; Herman, M.; Van Craen, J. C.; Colin, R. *J. Mol. Spectrosc.* **1982**, *95*, 101.

(4) Van Craen, J. C.; Herman, M.; Colin, R.; Watson, J. K. G. *J. Mol. Spectrosc.* **1985**, *111*, 185.
(5) Van Craen, J. C.; Herman, M.; Colin, R.; Watson, J. K. G. *J. Mol. Spectrosc.* **1986**, *119*, 137.
(6) Utz, A. L.; Tobiason, J. D.; Carrasquillo, M.; E.; Sanders, J. L.; Crim, F. F. *J. Chem. Phys.* **1993**, *98*, 2742.
(7) Tobiason, J. D.; Utz, A. L.; Crim, F. F. *J. Chem. Phys.* **1993**, *99*, 928.
(8) Tobiason, J. D.; Utz, A. L.; Sibert, E. L., III; Crim, F. F. *J. Chem. Phys.* **1993**, *99*, 5762.
(9) Fujii, M.; Tanabe, S.; Okuzawa, Y.; Ito, M. *Laser Chem.* **1993**, *14*, 79.
(10) Ochi, N.; Tsuchiya, S. *Chem. Phys. Lett.* **1987**, *140*, 20.
(11) Ochi, N.; Tsuchiya, S. *Chem. Phys.* **1991**, *152*, 319.
(12) Dupre, P.; Jost, R.; Lombardi, M.; Green, P. G.; Abramson, E.; Field, R. W. *Chem. Phys.* **1991**, *152*, 293.
(13) Dupre, P. *Chem. Phys.* **1995**, *196*, 239.
(14) Drabbels, M.; Heinze, J.; Meerts, W. L. *J. Chem. Phys.* **1994**, *100*, 165.
(15) Fujii, M.; Haijima, A.; Ito, M. *Chem. Phys. Lett.* **1988**, *150*, 380.
(16) Mordaunt, D. H.; Ashfold, M. N. R. *J. Chem. Phys.* **1994**, *101*, 2630.
(17) Mordaunt, D. H.; Ashfold, M. N. R.; Dixon, R. N.; Loffler, P.; Schnieder, L.; Welge, K. H. *J. Chem. Phys.* **1998**, *108*, 519.
(18) Wilson, S. H. S.; Read, C. L.; Mordaunt, D. H.; Ashfold, M. N. R.; Kawasaki, M. *Bull. Chem. Soc. Jpn.* **1996**, *69*, 71.
(19) Hashimoto, N.; Suzuki, T. *J. Chem. Phys.* **1996**, *104*, 6070.
(20) Shi, Y.; Suzuki, T. *J. Phys. Chem.* **1998**, *102*, 7414.
(21) Suzuki, T.; Hashimoto, N. *J. Chem. Phys.* **1999**, *110*, 2042.
(22) Cui, Q.; Morokuma, K.; Stanton, J. F. *Chem. Phys. Lett.* **1996**, *263*, 23.
(23) Cui, Q.; Morokuma, K. *Chem. Phys. Lett.* **1997**, *272*, 319.
(24) Lafferty, W. J.; Thibault, R. J. *J. Mol. Spectrosc.* **1964**, *68*, 183.
(25) Watson, J. K. J. *Mol. Phys.* **1968**, *15*, 479.
(26) Huber, D. *Int. J. Quantum Chem.* **1985**, *28*, 245.
(27) Dai, H. L.; Corpa, C. L.; Kinsey, J. L.; Field, R. W. *J. Chem. Phys.* **1985**, *82*, 1688.
(28) Utz, A. L. PhD Thesis, University of Wisconsin-Madison, 1992, Chapter 5.
(29) Sherill, C. D.; Yamaguchi, Y.; Schaefer, H. F., III; Stanton, J. F.; Gauss, J. *J. Chem. Phys.* **1996**, *104*, 8507.
(30) Drucker, S.; O'Brien, J. P.; Patel, P. O.; Field, R. W. *J. Chem. Phys.* **1997**, *106*, 3423.
(31) Humphrey, S. J.; Morgan, C. G.; Wodtke, A. M.; Cunningham, K. L.; Drucker, S.; Field, R. W. *J. Chem. Phys.* **1997**, *107*, 49.